Journal of Building Engineering 67 (2023) 105966

Contents lists available at ScienceDirect

Journal of Building Engineering

journal homepage: www.elsevier.com/locate/jobe

Full length article

The Vatic Weather File Generator (VWFG v1.0.0)

Amir A. Aliabadi *, Rachel M. McLeod

School of Engineering, University of Guelph, RICH 2515, Guelph, N1G 2W1, Ontario, Canada

ARTICLE INFO

Dataset link: https://github.com/AmirAAliabadi

Keywords:
Building performance
Statistical downscaling
Urban physics models
Weather files

ABSTRACT

To combat climate change caused by cities, it is necessary to perform urban physics modeling to assess mitigation solutions suitable for future climates. A challenge is availability of reliable future weather files for investigation of future climate scenarios. This research aims to develop the Vatic Weather File Generator (VWFG) using the statistical downscaling approach to fill this gap. VWFG is novel by using a history of weather files over multiple years to downscale future climate model data utilizing (1) quantile–quantile bias corrections, (2) record matching by the Finkelstein–Schafer method, and (3) shifting–stretching corrections. This implementation of VWFG uses the CanRCM4 climate model (1980–2100) and the ERA5 reanalysis data product as weather files (1980–2020) for two Representative Concentration Pathway (RCP) scenarios. VWFG outputs are consistent with findings in other studies. Further, to investigate the performance of VWFG for a case in Toronto, Canada, the Vertical City Weather Generator (VCWG) is forced by VWFG to predict the building sensible heating and cooling energy demands for a two-story single-family residential house. It is found that the building sensible heating demand is reduced over time (~ 15%–30% for RCP 4.5–8.5 Wm^{-2}) and the building sensible cooling demand is increased over time (~ 20%–50% for RCP 4.5–8.5 Wm^{-2}). The amount of change is greater for RCP 8.5 than RCP 4.5 Wm^{-2}. VWFG is a simple, practical, and widely applicable tool for urban physics simulations of future climates, particularly in cases where reliable forcing data is lacking otherwise.

1. Introduction

Designing and operating sustainable buildings require an understanding of future climate and weather conditions. Urban Physics Models (UPMs) (e.g. EnergyPlus and TRNSYS) are often used to assess different future scenarios (e.g. Special Report on Emissions Scenarios (SRES), Representative Concentration Pathways (RCP), or Shared Socio-economic Pathways (SSPs) [1]), when choosing building features for decarbonization, reliability, and resiliency. UPMs often require weather files (for instance in EnergyPlus Weather (EPW) or International Weather for Energy Calculations (IWEC) formats) for each region with at least hourly time resolution; however, most future regional/global climate models exhibit coarse spatial and temporal resolutions, so they cannot directly generate weather files.

Two major methods are used to produce future weather files at hourly time resolution: dynamical and statistical downscaling. Dynamical downscaling requires physical modeling of future weather, which produces high resolution and more reliable data, but it is computationally expensive and requires accurate representation of future boundary and initial conditions for the models at specified regions [2,3]. Statistical downscaling, on the other hand, is simpler and creates a statistical link between observed/reanalyzed local weather files and future weather datasets provided by regional or global climate models at coarse spatial

* Corresponding author.
E-mail address: aliabadi@uoguelph.ca (A.A. Aliabadi).
URL: https://www.aaa-scientists.com (A.A. Aliabadi).

https://doi.org/10.1016/j.jobe.2023.105966
Received 25 August 2022; Received in revised form 11 January 2023; Accepted 24 January 2023
Available online 1 February 2023

and temporal resolutions [4], but it cannot predict extreme weather conditions reliably [2,3]. Complete review of all downscaling methods is beyond the scope of this article, but few widely used statistical downscaling methods can be referred to below.

Belcher et al. [5] implemented one of the earlier statistical downscaling methods, titled morphing, to generate future weather files. This method used present or baseline weather files to adjust the monthly mean and standard deviation of baseline weather variables to those predicted by global climate models. A common morphing strategy is to construct a Typical Meteorological Weather (TMY) file based on a user-specified historical time window as the baseline for downscaling [6,7]. Widely popular platforms to generate future weather files based on morphing and statistical downscaling for UPMs are the CCWorldWeatherGen tool, WeatherShift^{TM}, and Meteonorm. These tools utilize a single climate model or an ensemble of climate models to predict future weather variables. They create either a single Typical Meteorological Year (TMY) file or additional eXtreme Meteorological Year (XMY) files. They may also apply corrections to the future weather variables [2–4,8,9].

Hosseini et al. [9] implemented one the latest statistical downscaling methods, which combined a hybrid regression and machine learning (classification) scheme. The method uses observed historical weather files and compares the weather variables with the outputs of a General Circulation Model (GCM) titled the Geophysical Fluid Dynamics Laboratory Coupled Model Earth System Model (GFDL-ESM2M). The method identifies the appropriate weighting parameters for combining a number of weather variables to match monthly GCM and observed weather files. It further identifies and removes any bias in the GCM variables based on the observed data. For cases that future GCM data are beyond the range of the observed data, the method also applies a correction. The downscaling method shows improvements in accuracy compared to a basic morphing method.

Few limitations remain in widely accepted methods that generate future weather files. Perhaps the greatest limitation is the inclusion of only a single Typical Meteorological Weather (TMY) file as the baseline for future downscaling, which misses multi-year and extreme weather variability [2,6,10]. Consideration of multi-year historical weather files is advantageous since such a dataset can capture extreme weather events, such as heat waves, and the natural inter-annual/decadal variability in climate conditions, such as the Atlantic Multi-decadal Oscillation (AMO) or the El Nino-Southern Oscillation (ENSO) [11]. Another limitation is lack of flexibility in the driving forcing datasets, which include both the sources for the baseline weather files and future regional/global climate models. For instance, Jentsch et al. [12] emphasizes the importance of the availability of specific regional climate models (over global climate models) for more accurate downscaling of weather files. Region-specific climate models implement more realistic boundary conditions and provide datasets at higher spatial and temporal resolutions. The third limitation is the simplicity of the method for general applicability.

Despite the available tools, there is need for a flexible open source software that can produce future weather files for UPMs. Such a tool shall (1) take any regional/global climate model with a daily time resolution as a future weather dataset, (2) take any observation- or reanalysis-based weather dataset to generate past weather files, (3) take any number of meteorological variables for statistical downscaling, by matching and correction of the future weather variables to those variables available in the past weather files, and (4) be simple to implement.

The main purpose of this article is to introduce such a tool, titled the Vatic Weather File Generator (VWFG), as a general purpose future weather file generator based on statistical downscaling. There are key differences between VWFG and other statistical downscaling approaches: (1) VWFG considers a history of weather files (as opposed to a single Typical Meteorological Year (TMY) file or addition of limited number of eXtreme Meteorological Year (XMY) files) and attempts to match future weather records to those of the past and perform bias correction of future weather records using past data toward creation of more accurate future weather files; (2) VWFG is flexible in the choice of the driving forcing datasets, number of years for analysis, and number of weather variables used for downscaling.

The structure of the article is as follows. Section 2 describes the methodology, involving preparation of the input datasets, the VWFG algorithm, and the introduction of the UPM that is forced with VWFG outputs. Section 3 provides the results and discussions, providing some statistical metrics (e.g. bias and root mean square error) to evaluate the performance of VWFG, providing quantitative future trends for meteorological variables studied, and providing quantitative building energy demands in the future for a sample building. Section 4 offers the conclusions and future work.

2. Methodology

VWFG is developed in Python 3.6. Below in Section 2.1 the input datasets to VWFG are discussed; in Section 2.2 the VWFG algorithm is introduced; and in Section 2.3 the UPM, the Vertical City Weather Generator (VCWG) is introduced, which is forced by the VWFG output for building energy load simulations.

2.1. Input datasets

Weather files associated with the historical/validation period(s) are prepared using the ERA5 dataset from the European Centre for Medium-Range Weather Forecasts (ECMWF). The ERA5 dataset provides the required variables for the EPW file format at an hourly resolution. The spatial horizontal resolution of the ERA5 dataset is 31 km. Quality-checked monthly updates of ERA5 dataset are available since 1979 until present, and they are published within three months of real time. ERA5 dataset combines historical observations into global estimates using advanced modeling and data assimilation systems [13]. For generation of historical/validation period(s) weather files, it may be preferred to use reanalysis data products, as opposed to pure observations, since reanalysis data are available at greater spatial and temporal resolutions with fewer data gaps. In a sense, reanalysis data can be regarded as *ground truth* for situations where the quality of weather observations are poor with possibly low spatial or temporal

Table 1
ERA5 variables used to prepare EPW files.

Data product	Variable names
ERA5Land	2 m Dew Point Temperature [°C]
ERA5Land	2 m Temperature [°C]
ERA5Land	Soil Temperature [°C]
ERA5Land	Wind [ms^{-1}]
ERA5Land	Pressure [Pa]
ERA5Land	Precipitation [mm]
ERA5	Total Sky Direct Solar Radiation at Surface [Wm^{-2}]
ERA5	Surface Solar Radiation Downwards [Wm^{-2}]
ERA5	Surface Thermal Radiation Downwards [Wm^{-2}]

resolutions. Despite the limitations, reanalysis data can be suitable for universal tools that attempt to perform statistical downscaling to generate weather files for building simulations.

Urban Physics Models (UPMs) are usually either forced at the top of the urban model domain or at the surface level in a rural area nearby a city. For instance, the Urban Weather Generator (UWG) is forced at a nearby rural site [14–17], while the Vertical City Weather Generator (VCWG) can be forced either on top of the urban domain or a nearby rural site [18–20].

VWFG considers surface level forcing. Once the specific latitude and longitude for forcing the UPM are selected, VWFG retrieves data from two "Reanalysis" products of ERA5.[1] These are "ERA5" and "ERA5Land". ERA5Land contains most of the data at high spatial resolution, except for a few radiative terms, which need to be downloaded from ERA5 at lower spatial resolution. These variables are listed in Table 1. For the present analysis the coordinates of data retrieval are given by latitude = 43.649889° and longitude = −80.121909°, associated with a rural site west of Toronto, Canada. The ERA5 data are downloaded in NetCDF format and assembled into EPW files for historical and validation periods.

For generation of future weather files, use of Regional Climate Models (RCMs) is preferred over Global Climate Models (GCMs). This is the case since RCMs are already one further step downscaled and supplied with more detailed initial and boundary conditions pertinent to a local region of interest [3,21]. In addition, if extreme climate events are to be accounted for, it may be preferable not to perform ensemble averaging of multiple RCMs but instead to rely on a single and accurate RCM that represents local climate conditions of a region [8].

The Working Group II (WGII) of the Sixth Assessment Report of the Intergovernmental Panel on Climate Change (IPCC) provides a framework for considering future climate scenarios [1]. WGII assesses the literature based on climate model simulations, which are part of the fifth and sixth Coupled Model Intercomparison Project (e.g. CMIP5, CMIP6) of the World Climate Research Programme. Future projections are made considering emissions and/or concentrations from Representative Concentration Pathways (RCPs) and Shared Socio-economic Pathways (SSPs) scenarios, respectively. However, earlier literature considers future climate scenarios based on the fifth Assessment Report (AR5), CMIP6, or other definitions. WGII considers the various literature and provides an integrated SSP-RCP framework to make future climate projections. For instance, SSP-RCP scenarios of 1.9, 2.6, 4.5, 7.0, and 8.5 are provided [1].

VWFG uses the Canadian Centre for Climate Modeling and Analysis Regional Climate Model (CanRCM4) to identify and utilize historical/validation/future period(s) climate variables under RCPs 4.5 and 8.5 Wm^{-2}. RCP 8.5 Wm^{-2} represents a business-as-usual scenario, while RCP 4.5 Wm^{-2} considers adoption of some mitigation measures in emissions [8]. CanRCM4[2] is available at a horizontal grid resolution of approximately 25 km over North America, and its parent global model is CanESM2. CanRCM4 was developed with the intention to downscale climate predictions and climate projections made by its parent global model. The novelty of the CanRCM4 stems from the philosophy of coordinating the deployment and application of the Regional Climate Model (RCM) in close connection with its parent Global Climate Model (GCM). For instance, both RCM and GCM in a coordinated paradigm adhere strictly to the same physics package [22]. VWFG retrieves the RCM data at a grid point that is closest to the latitude and longitude specified in the EPW dataset. VWFG uses four climate variables from CanRCM4. These are the mean daily temperature [K], surface wind speed [ms^{-1}], surface pressure [Pa], and total global horizontal radiation flux [Wm^{-2}]. A sample format of the CanRCM4 dataset is provided as

```
# 0: Day of Year [-] 1: lat [deg] 2: lon [deg] 3: tas [K]
# 4: sfcWind [m s-1] 5: ps [Pa] 6: rad [W m-2]
0  41.678688  283.323761  265.603729  2.334936  98599.953125  277.086670
1  41.678688  283.323761  267.726898  1.530065  98223.648438  301.935883
2  41.678688  283.323761  263.530579  1.622525  98564.757812  291.135010
3  41.678688  283.323761  264.215393  3.314878  98840.726562  292.283752
4  41.678688  283.323761  268.024506  3.666362  98211.281250  267.137665
5  41.678688  283.323761  269.779297  2.717463  98287.382812  329.165802
```

[1] https://cds.climate.copernicus.eu/ (Accessed 18 July 2022).
[2] https://climate-modelling.canada.ca/climatemodeldata/canrcm/CanRCM4/ (Accessed 18 July 2022).

An important assumption in the development of VWFG is that the regional Climate Model (CM) is stationary, which postulates that the biases in the CM are stationary or vary predictably [23]. In our case, it is desired that the CM biases do not vary with time in future climate scenarios for a specific location. This hypothesis, however, cannot be tested directly. It is suggested that violations of stationarity assumption can vary geographically, seasonally, and with the amount of projected climate change [24]. There are investigations showing examples both for and against the stationarity assumption [23–25].

2.2. Algorithm

Fig. 1 shows the process diagram of VWFG. Three sets of data are provided as input: (1) the weather files in the EnergyPlus Weather (EPW) format containing the hourly weather variables, which are retrieved from ERA5 reanalysis products; (2) the regional Climate Model (CM) variables containing the mean daily weather variables retrieved from the CanRCM4 regional climate model; and (3) the weighing factors to combine weather variables for matching CM records to EPW files.

The diagram shows three time periods for the process flow: (1) the historical time period (1980–1999); (2) the validation time period (2007–2020); and (3) the future time period (2021–2100). It must be noted that the quality control of the ERA5 data suggests that the reanalysis products are not reliable in the time period (2000–2006) [13]. Therefore this time period is excluded from the process flow, i.e. there is a data gap from 2000 to 2006.

The overall algorithmic process is described in this paragraph, while the detailed processes are described in the subsequent paragraphs. For the historical time period, the Quantile–Quantile (Q–Q) method is used to identify the bias in historical CM records with respect to the historical EPW records. The historical time period is also used to compute the monthly mean and standard deviation of four weather variables discussed earlier in the historical EPW records. For the validation period, the Q–Q method is used to remove the bias from the validation CM records. Then the Finkelstein–Schafer (F–S) statistic is used on a Q–Q basis to match the validation CM records to the corresponding historical EPW records for downscaling. Further, the monthly mean and standard deviation of four weather variables discussed earlier are computed. The pair of means and standard deviations in the validation CM record and the matching historical EPW record enable correcting the created validation EPW record (downscaled validation CM records) by shifting and stretching the distribution for each of the four weather variables. At the end of the calculations for the validation period, it is possible to perform error analysis to find out if the bias correction or the shift–stretch methods improve the performance of the downscaling process. This is possible because there are reference validation EPW records for comparison to the created EPW records (downscaled validation CM records). The error analysis computes the bias and Root Mean Square Error ($RMSE$) for the four meteorological variables by comparing the downscaled values to the reference validation values. For the future period, similar Q–Q bias correction, Q–Q F–S match, and shift–stretch methods are performed to downscale the future CM records into future EPW records. There are no reference values for the future period, so no error analysis is possible; however, having the error analysis associated with the validation period increases the confidence in the downscaling method.

The Quantile–Quantile (Q–Q) method is an adjustment made to projected regional/global climate model datasets to identify and remove the model bias with respect to a reference dataset [26]. For downscaling of climate model data to produce weather files, the method sorts each of the mean diurnal weather variables in a month and produces a Cumulative Distribution Function (CDF). For each daily quantile, the shift of this CDF with respect to the reference CDF defines the bias. Thus, the bias for daily quantile i over a sample of j monthly records is defined as

$$B(i) = \frac{1}{N}\sum_{j=1}^{N}(X_{\mathrm{CM},i,j} - X_{\mathrm{EPW},i,j}), \tag{1}$$

where X refers to each of the four variables of mean daily temperature [K], surface wind speed [ms^{-1}], surface pressure [Pa], and total global horizontal radiation flux [Wm^{-2}]. Ideally $N \gg 1$ so that many identical months are considered for calculation of the bias. For instance, if historical records over 20 years are considered ($N = 20$), for each month the bias for daily quantile i is computed taking the average of 20 shifts.

The Finkelstein–Schafer (F–S) statistic is also defined on a Q-Q basis, but in this statistic the absolute value of the difference between the validation or future CM value and the historical EPW value for each quantile is averaged over all quantiles. The F-S statistic is defined as

$$FS_X = \frac{1}{n}\sum_{i=1}^{n}|X_{\mathrm{CM},i} - X_{\mathrm{EPW},i}|, \tag{2}$$

where n is the number of bins (days) in the CDF. To match future and historical records, a number of meteorological variables must be selected with appropriate weights to construct a weighted sum statistic. Two conditions are important in deciding the variables and the weights: (1) the variables chosen must be the least correlated among one another; and (2) the weights should be increased for variables that have the highest impact on the building performance metrics under consideration [9,11,27]. For instance, to determine the building energy demand, temperature has the greatest impact, followed by pressure, global horizontal radiation flux, and wind speed. The weighted sum to be minimized for a match is given by

$$WS = w_{\mathrm{T}}FS_{\mathrm{T}} + w_{\mathrm{P}}FS_{\mathrm{P}} + w_{\mathrm{R}}FS_{\mathrm{R}} + w_{\mathrm{S}}FS_{\mathrm{S}}. \tag{3}$$

VWFG requires the user to know, *apriori*, the importance of the weather variables and the associated weights. The weights for dry bulb temperature T [K], w_{T}, pressure P [Pa], w_{P}, global horizontal radiation flux R [Wm^{-2}], w_{R}, and wind speed S [ms^{-1}],

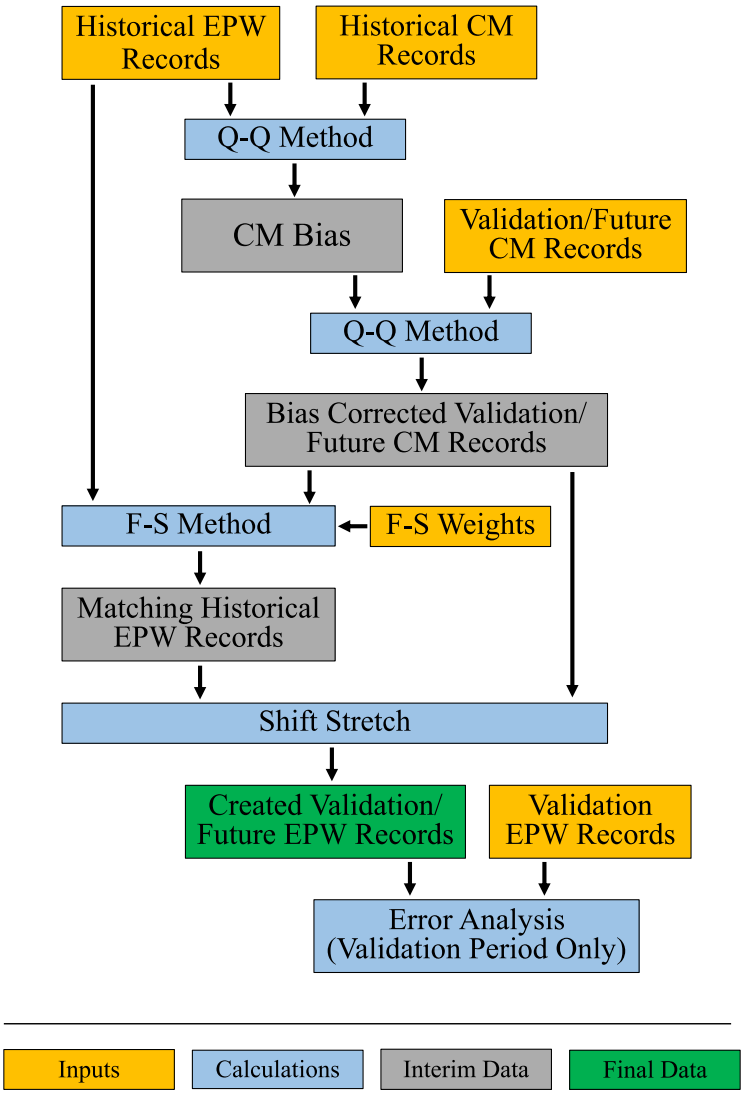

Fig. 1. The process diagram for the Vatic Weather File Generator (VWFG); EnergyPlus Weather (EPW) files produced by ERA5 data; Climate Model (CM) files produced by the CanRCM4 model; Quantile–Quantile (Q–Q) method; Finkelstein-Schafer (F–S) method; Finkelstein–Schafer (F-S) weights.

Table 2
Weighing factors for meteorological variables in Toronto [9].

Month	Dry bulb temperature	Pressure	Radiation	Wind speed
January	0.773	0.086	0.078	0.063
February	0.912	0.036	0.027	0.026
March	0.891	0.041	0.036	0.032
April	0.884	0.043	0.038	0.036
May	0.869	0.052	0.043	0.036
June	0.887	0.048	0.037	0.028
July	0.830	0.064	0.057	0.048
August	0.868	0.057	0.045	0.030
September	0.829	0.068	0.054	0.048
October	0.831	0.060	0.056	0.053
November	0.905	0.039	0.031	0.025
December	0.922	0.027	0.026	0.026

w_S, are provided by Hosseini et al. [9,27], who used classification methods based on machine learning to find the variables meeting the weighted sum criteria mentioned above. Table 2 shows the weighing factors used by VWFG.

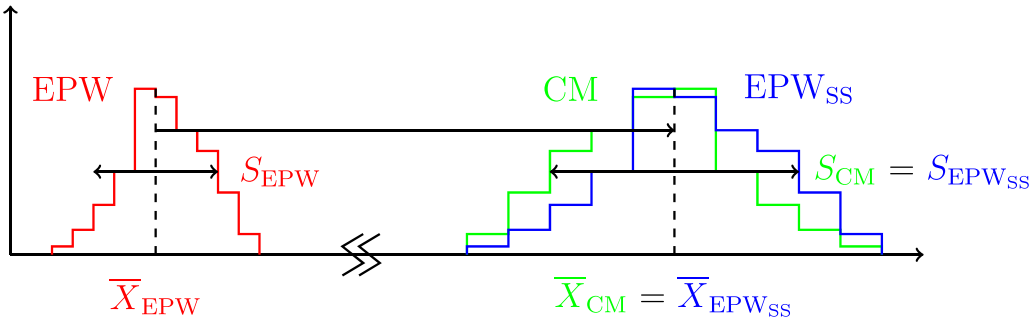

Fig. 2. The shift and stretch method adjusts the EnergyPlus Weather (EPW) record (red) to the Climate Model (CM) record (green) so that the modified EPW record (blue) exhibits the same mean and standard deviation ($\overline{X}_{EPW_{SS}}$, $S_{EPW_{SS}}$) as the CM record ($\overline{X}_{CM}$, S_{CM}); each distribution is associated with mean daily values of meteorological variables for one month. (For interpretation of the references to color in this figure legend, the reader is referred to the web version of this article.)

The shift and stretch method is demonstrated in Fig. 2 . It adjusts the average and standard deviation of the created validation or future EPW record to those of validation or future CM record, respectively [5]. Since the validation or future CM record only provides mean daily values of meteorological variables, the created validation or future EPW record is first averaged to produce mean daily values of the same variables, and then the mean and standard deviation of the variables are used for the shift and stretch method via

$$X_{EPW_{SS}} = \overline{X}_{CM} + \left(X_{EPW} - \overline{X}_{EPW}\right)\frac{S_{CM}}{S_{EPW}}, \tag{4}$$

where $X_{EPW_{SS}}$ is the adjusted record, $\overline{X}_{CM}$ is the mean daily value of the meteorological variable in the validation or future CM record, $\overline{X}_{EPW}$ is the mean daily value of the created validation or future EPW record, S_{CM} is the standard deviation of daily value in the validation or future CM record, and S_{EPW} is the standard deviation of the daily value in the created validation or future EPW record. Note that each distribution represents one month, and twelve corrections are needed to adjust a full year of data.

2.3. Urban physics model

To demonstrate the utility of the statistical downscaling method, the resulting future climate EPW weather files are used as boundary and forcing conditions for a UPM titled the Vertical City Weather Generator (VCWG) [18–20]. VCWG is a computationally-fast UPM that predicts temporal and vertical variation of meteorological variables in the urban environment, building envelope temperatures, and temporal variation of building performance metrics, such as indoor air temperature, indoor specific humidity, building thermal and electricity loads, and natural gas and electricity consumptions [19]. Various versions of VCWG are available. VCWG v1.3.2 is the original version [19]. It was enhanced with renewable and alternative energy integration in VCWG v1.4.5 and v1.4.6 [18]. The key difference between v1.4.5 and v1.4.6 is that v1.4.5 requires use of all renewable and alternative energy components, while v1.4.6 allows for utilization of solar photovoltaics and wind energy only, in addition to permitting an overall simulation including solar thermal energy, energy storage, heat pumps, and phase change materials. In this analysis VCWG v1.4.6 is used without the consideration of any renewable or alternative energy. VCWG v2.0.0 is the latest version so far, which includes hydrological processes [20] in addition to the base model features of VCWG 1.3.2.

As shown in Fig. 3, VCWG is composed of many sub-models: a rural model, a one-dimensional urban vertical diffusion model, a radiation model, and a building energy model. VCWG is forced with weather data from a rural site at the vicinity of the urban area in Toronto, Canada. This dataset is the outcome of the VWFG from 2021 to 2100 for two RCP scenarios (4.5 and 8.5 Wm^{-2}). The rural model is used to solve for the vertical profiles of meteorological variables and friction velocity at 10 m a.g.l. The rural model also calculates a horizontal pressure gradient. The rural model outputs are forced on the urban vertical diffusion model that solves vertical transport equations for meteorological variables. This vertical diffusion model is linked to the radiation and building energy models using feedback interaction. The effects of buildings and vegetation are considered. The two-way interaction coupling scheme among the sub-models is designed to update the boundary conditions, surface temperatures, and the source/sink terms in the transport equations in successive time step iterations. This is known as “ping-pong” coupling.

In this study the building archetype is a two-story single-family residential building. Table 3 shows the input parameters associated with the simulations in residential areas of Toronto. The input parameters are informed by previous field campaigns and simulations in south-western Ontario [18,28–30].

3. Results and discussion

Section 3.1 provides the Cumulative Distribution Functions (CDFs) for the meteorological variables and demonstrates the success of VWFG in matching a sample record from the validation period to one of the historical periods. Section 3.2 visualizes the matching

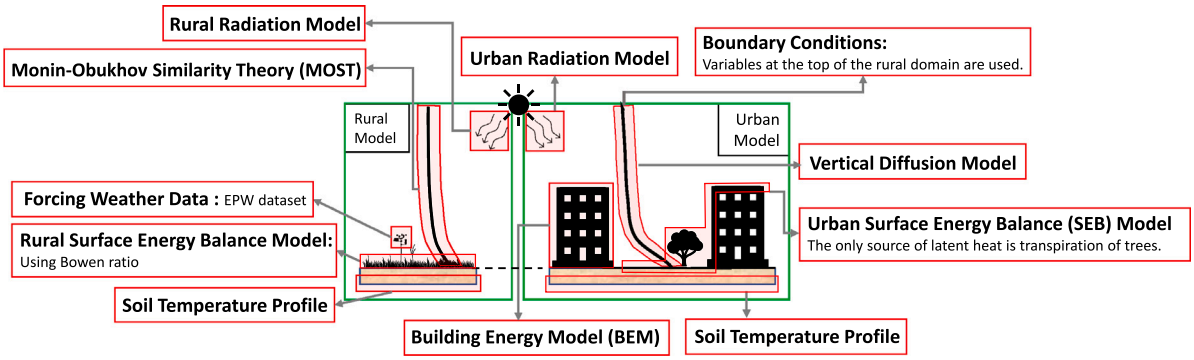

Fig. 3. Overview of the Vertical City Weather Generator (VCWG v1.4.6) model and the integration of sub-models.

Table 3
List of input parameters used in VCWG.

Parameter	Symbol	Value
Latitude [°N]	lat	43.732
Longitude [°W]	lon	79.573
Average buildings height [m]	H_{avg}	6
Width of canyon [m]	$w_x = w_y = w$	23
Building width to canyon width ratio [–]	$b_x/w_x = b_y/w_y = b/w$	0.42
Leaf Area Index [m^2 m^{-2}]	LAI	0–1
Tree trunk height [m]	h_t	3.6
Tree crown radius [m]	r_t	1.8
Tree distance from wall [m]	d_t	5
Ground vegetation cover fraction	δ_s	0.5
Building type	–	Mid rise apartment
Urban albedos (roof, ground, wall, vegetation) [–]	$\alpha_R, \alpha_G, \alpha_W, \alpha_V$	0.22, 0.125, 0.225, 0.225
Urban emissivities (roof, ground, wall, vegetation) [–]	$\epsilon_R, \epsilon_G, \epsilon_W, \epsilon_V$	0.95, 0.95, 0.95, 0.95
Rural overall albedo [–]	α_{rur}	0.2
Rural overall emissivity [–]	ϵ_{rur}	0.95
Rural aerodynamic roughness length [m]	$z_{0rur} = 0.1h_{rur}$	0.2
Rural roughness length for temperature [m]	$z_{\overline{\Theta},rur} = 0.1z_{0rur}$	0.02
Rural roughness length for specific humidity [m]	$z_{\overline{Q},rur} = 0.1z_{0rur}$	0.02
Rural zero displacement height [m]	$d_{rur} = 0.5h_{rur}$	1
Rural Bowen ratio [–]	β_{rur}	1.5
Ground aerodynamic roughness length [m]	z_{0G}	0.02
Roof aerodynamic roughness length [m]	z_{0R}	0.02
Vertical resolution [m]	Δz	1
Time step [s]	Δt	60
Canyon axis orientation [°N]	θ_{can}	45

months from the historical records that best agree with future records. Section 3.3 quantifies the bias reduction in the climate model records as a result of the bias correction procedure. It also quantifies the effect of shifting and stretching procedure on the errors in the weather file records. Sections 3.4 and 3.5 quantify the time series for the selected meteorological variables and temperature trends. They also compare the findings to other studies in the literature. Section 3.6 investigates a sample building's heating and cooling demands simulated using the output of the VWFG tool.

3.1. Cumulative distribution functions

Fig. 4 shows the CDFs of the four meteorological variables discussed earlier. The CDFs are constructed by considering mean daily values of each variable. Each CDF is associated with one month of data. The gray curves belong to historical EPW records, where all prior CDFs are plotted over the historical period (1980–1999). The blue curve is a sample validation CM record from the validation period (December 2009), and the red curve is the matched record from historical EPW weather files that is chosen using the F-S method. It can be seen that the CDFs match more closely for temperature, given the fact that the weighing factor for temperature is the highest, while the CDFs match less closely for other meteorological variables.

3.2. Matching months for future climate

It is interesting to investigate which months from the historical period match with which months in the future period. For instance, would a January always be matched with a January? or could a January also be matched with a December or any other

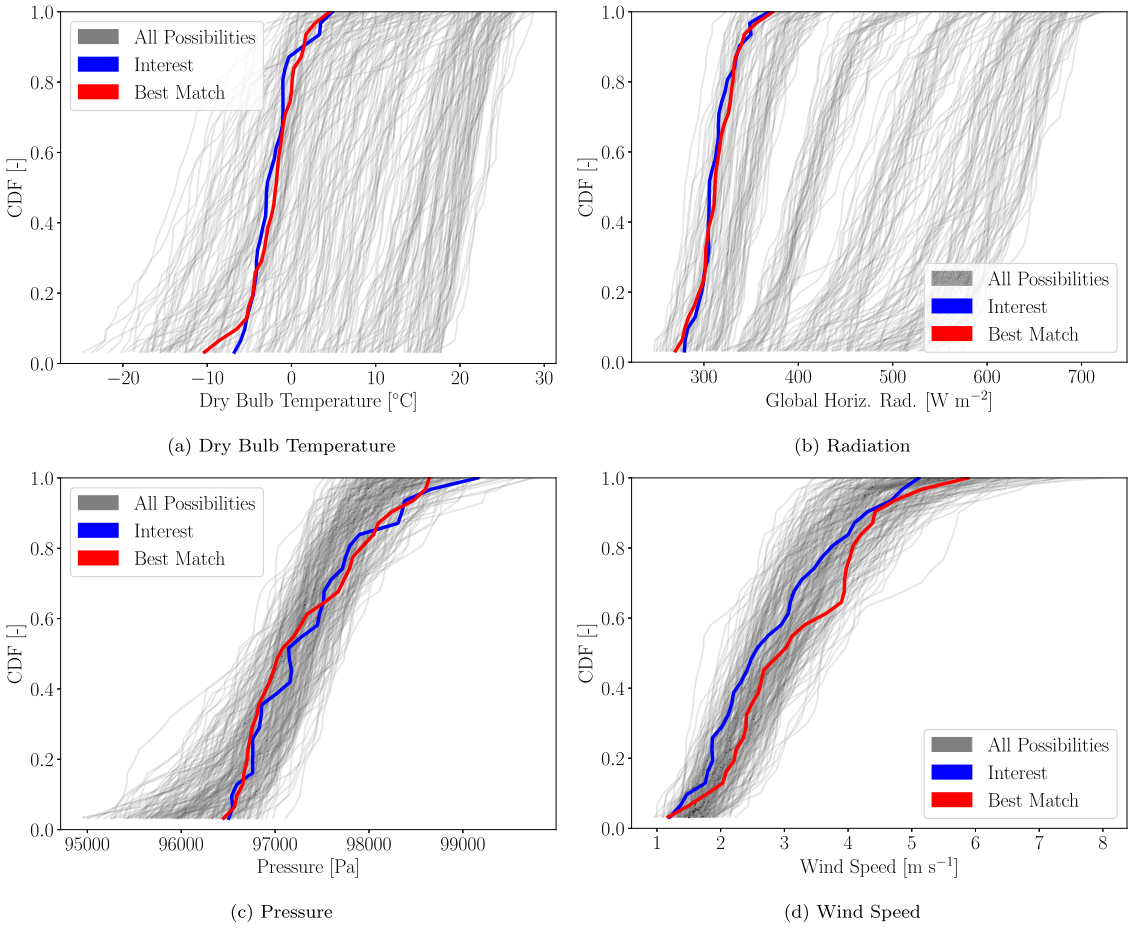

Fig. 4. Cumulative Distribution Functions (CDFs) for (a) dry bulb temperature, (b) radiation, (c) pressure, and (d) wind speed; all historical EnergyPluse Weather (EPW) weather file records in gray; sample validation Climate Model (CM) record to match in blue (December 2009); matching historical EPW record in red (December 1997); results for Toronto under RCP 4.5 Wm^{-2} climate scenario. (For interpretation of the references to color in this figure legend, the reader is referred to the web version of this article.)

month that also has 31 days? Fig. 5 visualizes the matching months for the future period from the historical EPW records. The vertical axis in the color plot shows future years, the horizontal axis shows the future months, and the color bar shows the historical months. The color plots are provided for the two RCP scenarios analyzed (4.5 and 8.5 Wm^{-2}).

Two factors influence the patterns for matching months: (1) the number of days in a month and (2) the similarity of meteorological conditions. For instance, it can be seen that only historical Februaries match future Februaries, given that only February has 28 days. For other months, it can be seen that the *shoulder* months can also match with one another, in addition to the same month. For instance, a future March (31 days) can match with a historical March as well as a historical October (31 days), which is a shoulder month for March. It can be speculated that with warming trends, distant future winter months may be matched by historical spring or fall months, or that distant future spring or fall months may be matched by historical summer months. For example, a future warm January may match with a historical March or October. However, for the period of analysis until 2100, this situation is not predicted. Perhaps, with time horizons much beyond 2100, the shifting patterns in the matching months may be encountered. As far as the two RCP scenarios are concerned, there is no particular difference for the month matching patterns between the two color plots.

3.3. Error reduction in climate model and weather files

It is desirable to investigate if the statistical techniques used actually improve the downscaling method. Notably, the validation period (2007–2020) can be used (1) to compare the bias-corrected validation CM records to the non-bias-corrected validation CM records and (2) to compare the created stretched-shifted validation EPW records to the created non-stretched-shifted validation EPW records. The RCP case of 4.5 Wm^{-2} is used for this analysis.

We begin this investigation for the bias correction of the validation CM records. Fig. 6 shows the CDFs of the validation CM bias in dry bulb temperature with and without bias correction. For reference, the zero bias line is plotted using a gray vertical line. The

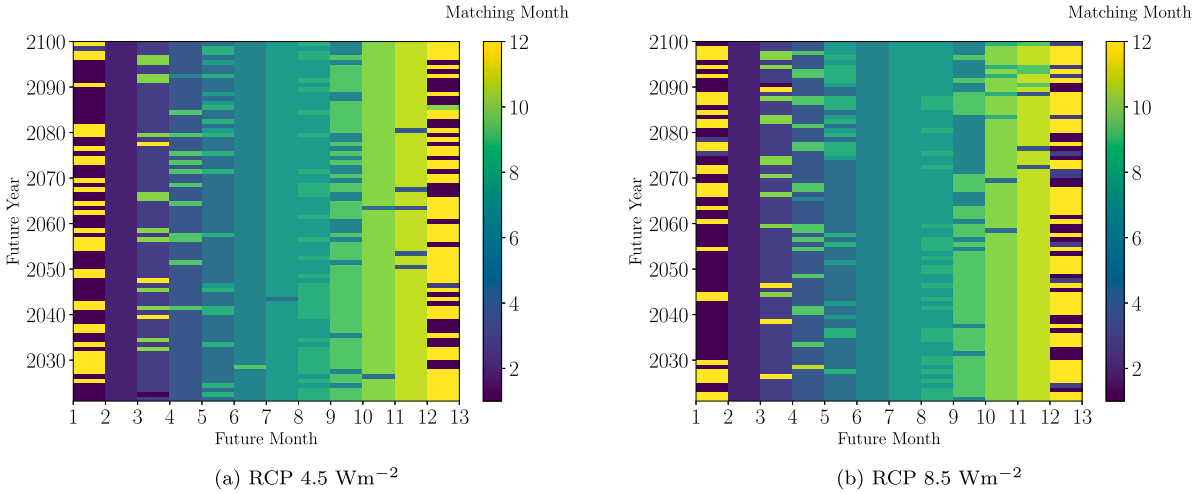

Fig. 5. Future climate matching months for (a) RCP 4.5 Wm^{-2} and (b) RCP 8.5 Wm^{-2}; color bar showing the months in the historical EnergyPlus Weather (EPW) weather file records, chosen to match future Climate Model (CM) records. (For interpretation of the references to color in this figure legend, the reader is referred to the web version of this article.)

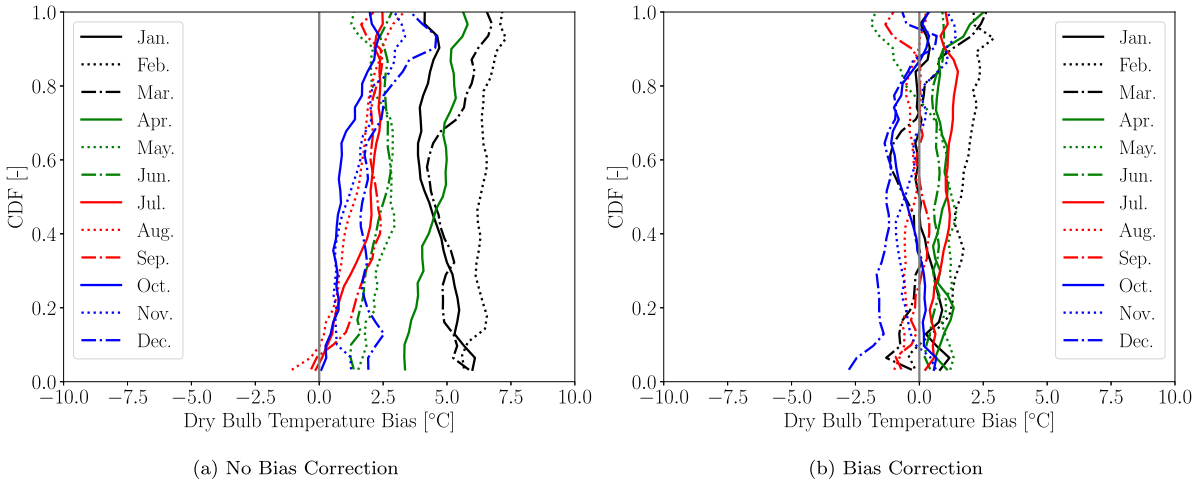

Fig. 6. Cumulative Distribution Functions (CDFs) for the bias of dry bulb temperature in the validation Climate Model (CM) records compared to validation EnergyPlus Weather (EPW) weather file records for the validation period using RCP 4.5 Wm^{-2} for (a) no bias correction and (b) bias correction cases.

non-bias-corrected records show that the temperature is mostly positively biased in the winter months followed by less positively biased temperatures in other seasons. Overall, temperatures are biased from 0 to 5 °C given the quantile and month of interest. The bias correction procedure results in reduced biases, so that the CDFs move to the left and reach closer to the zero bias line.

Fig. 7 shows the CDFs of the validation CM bias in pressure with and without bias correction. Similar to the temperature bias, the non-bias-corrected records show that the pressure is entirely positively biased by about 1000 to 2000 Pa, and the bias correction procedure results in reduced biases, so that the CDFs move to the left and reach closer to the zero bias line.

Fig. 8 shows the CDFs of the validation CM bias in global horizontal radiation flux with and without bias correction. Similar to the temperature and pressure biases, the non-bias-corrected records show that the radiation flux is entirely positively biased by about 0 to 75 Wm^{-2}, and the bias correction procedure results in reduced biases, so that the CDFs move to the left and reach closer to the zero bias line.

Fig. 9 shows the CDFs of the validation CM bias in wind speed with and without bias correction. Unlike temperature, pressure, and radiation flux, the non-bias-corrected records do not show a systematic shift toward positive or negative biases. Nevertheless, the bias correction procedure accumulates the CDFs closer to the zero bias line, except for the highest quantiles, which indicate very high wind speeds. It must be noted that wind patterns are very sensitive to the resolution, topography, and land use conditions of the driving reanalysis data product or climate model [31–35]. Such conditions can change over the period of few decades that specify the historical and validation time periods. Therefore, the success of the bias reduction procedure is more difficult to interpret. However, given the shape of the CDFs, there is evidence that the bias correction procedure improves the downscaling method.

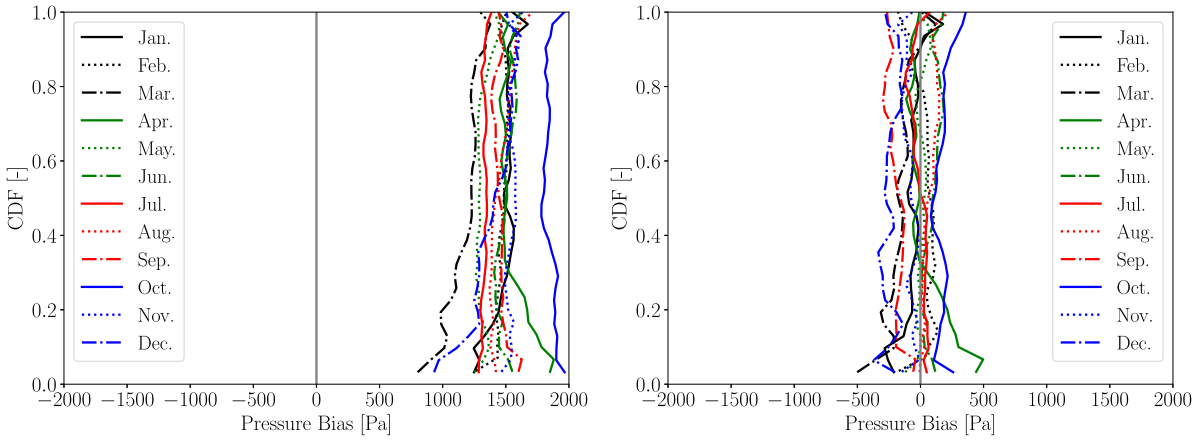

(a) No Bias Correction (b) Bias Correction

Fig. 7. Cumulative Distribution Functions (CDFs) for the bias of pressure in the validation Climate Model (CM) records compared to validation EnergyPlus Weather (EPW) weather file records for the validation period using RCP 4.5 Wm^{-2} for (a) no bias correction and (b) bias correction cases.

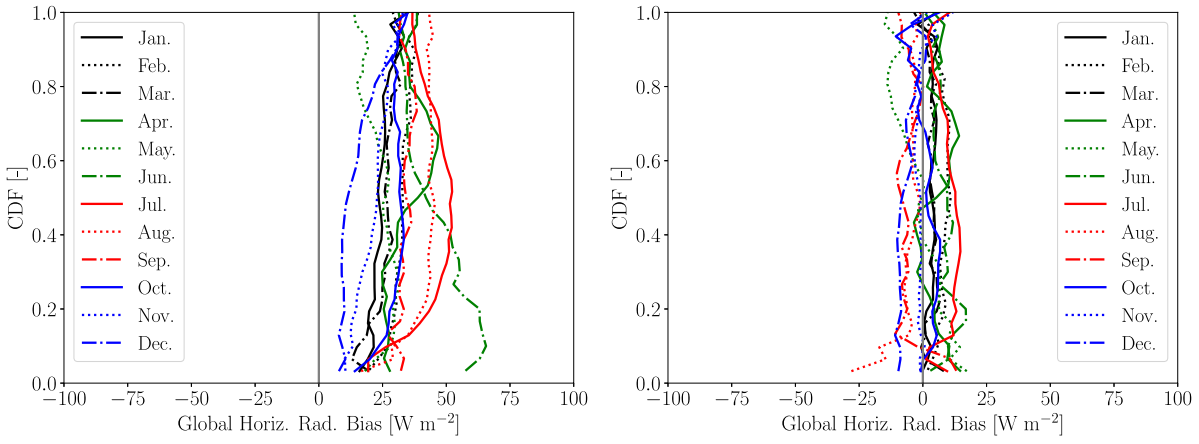

(a) No Bias Correction (b) Bias Correction

Fig. 8. Cumulative Distribution Functions (CDFs) for the bias of global horizontal radiation flux in the validation Climate Model (CM) records compared to validation EnergyPlus Weather (EPW) weather file records for the validation period using RCP 4.5 Wm^{-2} for (a) no bias correction and (b) bias correction cases.

We can next assess the impact of the stretching–shifting method on reducing the errors in the created validation EPW records for the validation period. Table 4 shows the computed biases and Root Mean Square Errors ($RMSE$s) before and after the shifting–stretching procedure is applied to the created validation EPW records for the validation period. The averages of the biases and $RMSE$s are also provided. It can be seen that no statistically notable change can be predicted. This is likely due to the fact that the validation period is only one decade apart from the historical period, and for all matches, distributions of the weather variables in both validation and historical periods have similar means and standard deviations. However, the shift–stretch method is crucial to keep in the downscaling process since future decades by the end of century will likely be associated with large temperature shifts compared to historical records. This point will be elucidated in Section 3.4.

3.4. Future climate time series

The downscaled future EPW weather files can be analyzed from 2021 to 2100. Both RCP scenarios of 4.5 and 8.5 Wm^{-2} can be considered. Figs. 10 to 13 show the time series of dry bulb temperature, pressure, global total horizontal radiation flux, and wind speed. Four selected months of January, April, July, and October are chosen for demonstration. In each figure, the markers show the monthly average and the shaded area shows one standard deviation of the monthly weather variables in the created future EPW records. The most notable figure with a clear trend is Fig. 10 for temperature. Overall, temperatures for all months and both RCP scenarios increase, except for a temporary decade of cooling in 2090 s. It can be noted that the warming trend is more accelerated for the RCP 8.5 Wm^{-2} scenario. This point will be further elucidated in Section 3.5.

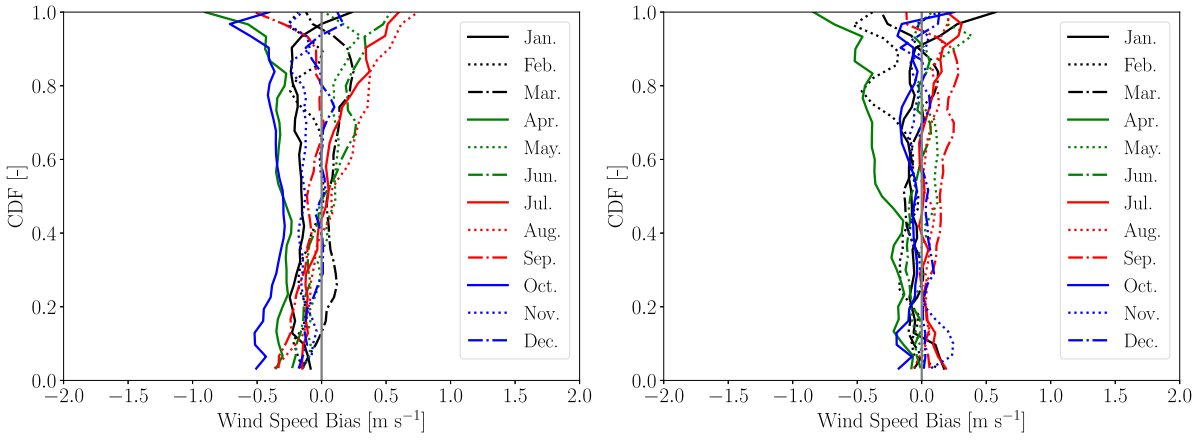

Fig. 9. Cumulative Distribution Functions (CDFs) for the bias of wind speed in the validation Climate Model (CM) records compared to validation EnergyPlus Weather (EPW) weather file records for the validation period using RCP 4.5 Wm^{-2} for (a) no bias correction and (b) bias correction cases.

Table 4
Table of biases (B) and Root Mean Square Errors ($RMSE$s) showing the effect of shifting and stretching method on the created validation EnergyPlus Weather (EPW) weather file records for RCP 4.5 Wm^{-2}.

Error statistic	B	B	B	B	$RMSE$	$RMSE$	$RMSE$	$RMSE$
Variable	T	P	R	S	T	P	R	S
Units	[°C]	[Pa]	[Wm^{-2}]	[ms^{-1}]	[°C]	[Pa]	[Wm^{-2}]	[ms^{-1}]
	No shift-stretch							
January	0.78	−54	−0.28	−0.07	8.59	1334	73	2.00
February	0.67	60	2.50	−0.26	9.30	1230	95	1.94
March	0.20	−117	−1.93	−0.09	8.27	1133	130	1.90
April	2.12	78	−0.72	−0.25	8.17	1120	167	1.92
May	0.41	31	−11.28	0.02	6.72	854	175	1.72
June	0.45	138	1.37	−0.04	5.20	776	158	1.61
July	0.20	29	−2.79	0.01	4.47	552	135	1.48
August	−0.98	100	−6.02	−0.01	4.34	660	128	1.44
September	−0.87	−151	−12.5	0.09	5.37	819	126	1.63
October	−1.07	189	−3.85	−0.20	5.70	1003	104	1.85
November	0.11	−83	−2.12	0.08	6.82	1122	77	2.01
December	−1.34	−131	−2.98	0.05	7.02	1176	65	1.92
Average	0.05	7	−3.38	−0.06	6.66	982	119	1.79
	Shift-stretch							
January	0.24	−68	3.33	−0.02	8.60	1357	80	1.97
February	1.56	23	6.86	−0.15	9.39	1219	103	1.89
March	−0.04	−163	3.24	−0.05	8.56	1176	139	1.92
April	0.92	47	2.69	−0.30	7.73	1135	187	1.89
May	0.58	1.91	−0.43	0.06	6.39	873	177	1.77
June	0.68	107	7.99	−0.04	5.48	786	169	1.64
July	0.92	2	10.20	0.07	4.48	562	149	1.57
August	−0.41	73	−6.36	0.071	4.69	663	150	1.47
September	−0.13	−173	−3.48	0.11	5.51	816	137	1.64
October	−0.20	174	1.75	−0.09	5.83	1063	108	1.89
November	0.07	−98	−0.33	0.03	6.83	1142	85	1.97
December	−1.23	−226	−6.39	0.03	6.94	1231	72	1.89
Average	0.25	−25	1.59	−0.02	6.70	1002	130	1.79

3.5. Dry bulb temperature trends

The temperature trends can be further analyzed by fitting lines to the time series and computing the warming rate for each month and each RCP scenario [36]. Table 5 shows the warming trends. Overall, the RCP 8.5 Wm^{-2} scenario shows accelerated warming compared to the RCP 4.5 Wm^{-2} scenario for all the months. Under the RCP 4.5 Wm^{-2} scenario, the rate of warming is the greatest for August (0.033 °Cyear^{-1}), September (0.035 °Cyear^{-1}), and October (0.03 °Cyear^{-1}). Similarly, under the RCP 8.5 Wm^{-2}

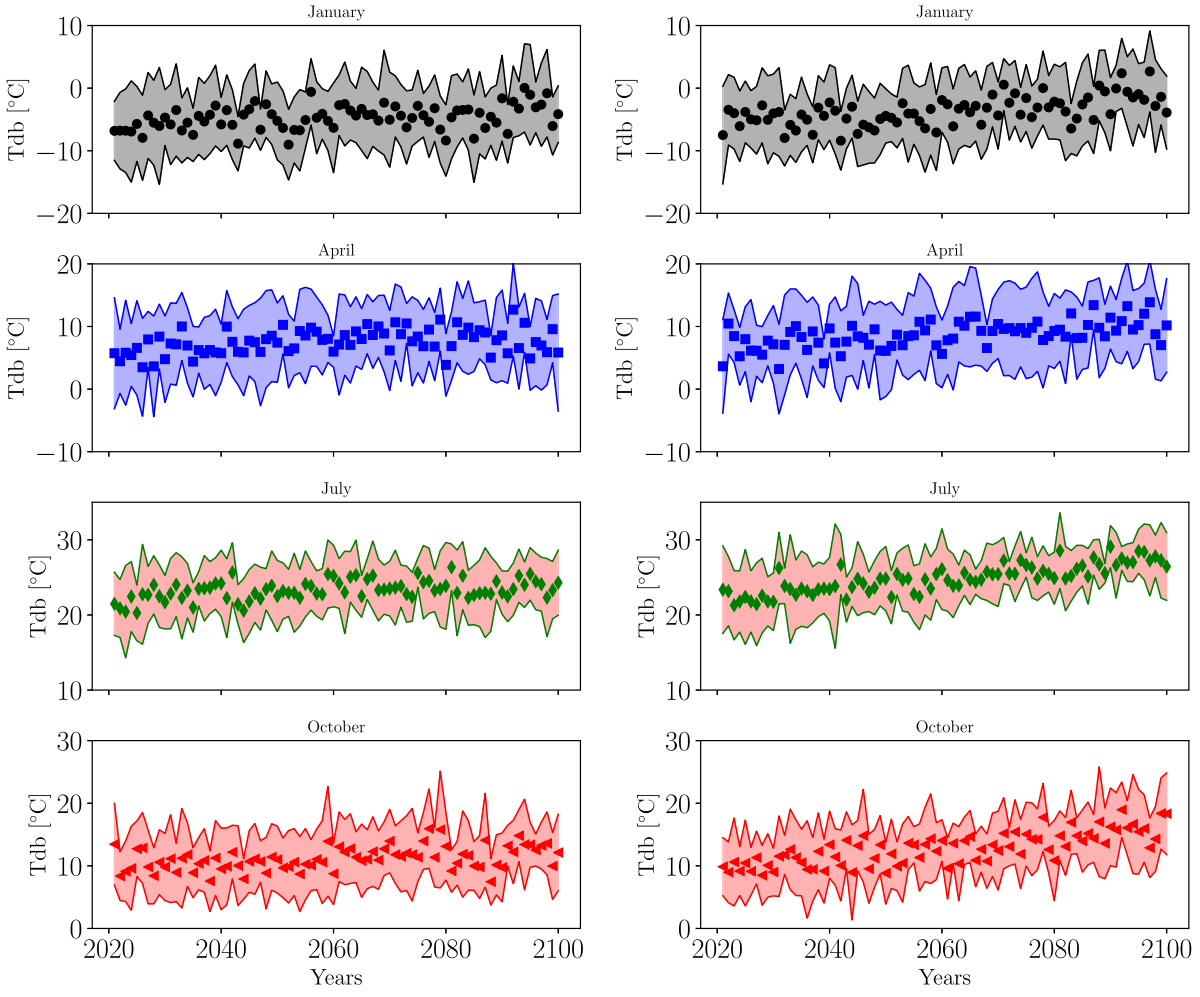

Fig. 10. Future climate temperature time series for (a) RCP 4.5 Wm^{-2} and (b) RCP 8.5 Wm^{-2}; the markers and shaded region showing the mean and one standard deviation, respectively, for annual daily values produced by the created future EnergyPlus Weather (EPW) weather file; showing selected months of January, April, July, and October.

scenario, the rate of warming is the greatest for August (0.079 °Cyear^{-1}), September (0.067 °Cyear^{-1}), and October (0.085 °Cyear^{-1}). On average, the annual rate of warming for RCPs 4.5 and 8.5 Wm^{-2} are 0.027 °Cyear^{-1} and 0.062 °Cyear^{-1}, respectively.

These temperature trends can be compared against those provided in the recent IPCC report and other studies. For instance, global temperature rise from 2021 to 2100 for RCP 4.5 and 8.5 Wm^{-2} scenarios are predicted as 1.5 °C and 3.5 °C, respectively [1]. On a per year basis, these values are 0.019 °Cyear^{-1} and 0.044 °Cyear^{-1}, respectively. As suggested by the IPCC report, most Canadian cities, including Toronto, will experience a warming rate greater than the global average.

A study by D'Agostino et al. [7] reports observed rates of warming for various European cities, including Milan, Italy, which is located at a similar latitude to Toronto. For Milan, a warming rate of 0.056 °Cyear^{-1} in the period 1973–2018 is measured, which is also lower to the rate of warming under the RCP 8.5 Wm^{-2} scenario for Toronto. The same study used the morphing approach and the WeatherShift^{TM} tool to predict the future weather conditions in 2060 under the RCP 8.5 Wm^{-2} scenario in Milan, Italy [10]. The predicted rate of warming until 2060 is 0.080 °Cyear^{-1}, which is higher than that predicted by VWFG in Toronto.

Comparing the temperature trends provided by VWFG and the studies reported above suggests that the rate of warming in Toronto is greater than the globally predicted rate of warming and comparable to the rate of warming in other locations of similar latitude. These results provide confidence in the skill of the VWFG to perform statistical downscaling of future climate records into weather files.

3.6. Building energy demands under future climate

Fig. 14 shows the projected building sensible heating and cooling demands from the present time until 2100 predicted by VCWG every decade. Both RCP 4.5 and 8.5 Wm^{-2} scenarios are considered. Overall, the building sensible heating demand is reduced

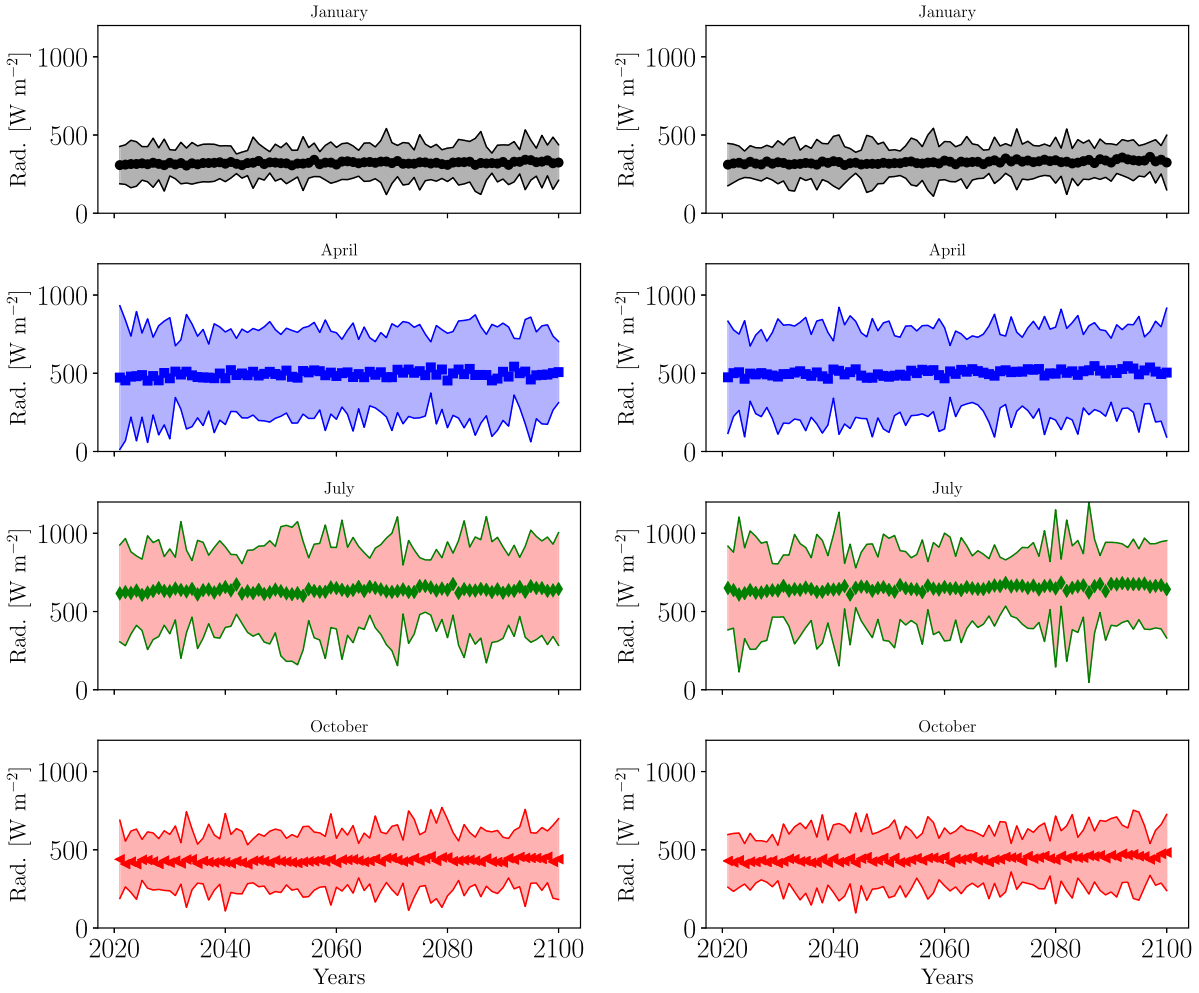

(a) RCP 4.5 Wm^{-2} (b) RCP 8.5 Wm^{-2}

Fig. 11. Future climate radiation flux time series for (a) RCP 4.5 Wm^{-2} and (b) RCP 8.5 Wm^{-2}; the markers and shaded region showing the mean and one standard deviation, respectively, for annual daily values produced by the created future EnergyPlus Weather (EPW) weather file; showing selected months of January, April, July, and October.

Table 5
Dry bulb temperature trends [°Cyear^{-1}] from 2021 to 2100 in Toronto under RCP 4.5 and 8.5 Wm^{-2} scenarios.

Month	Trend [°Cyear^{-1}] RCP 4.5 Wm^{-2}	Trend [°Cyear^{-1}] RCP 8.5 Wm^{-2}
January	0.031	0.057
February	0.030	0.064
March	0.031	0.041
April	0.029	0.052
May	0.020	0.063
June	0.016	0.066
July	0.023	0.067
August	0.033	0.079
September	0.035	0.067
October	0.032	0.085
November	0.018	0.053
December	0.021	0.047
Average	0.027	0.062

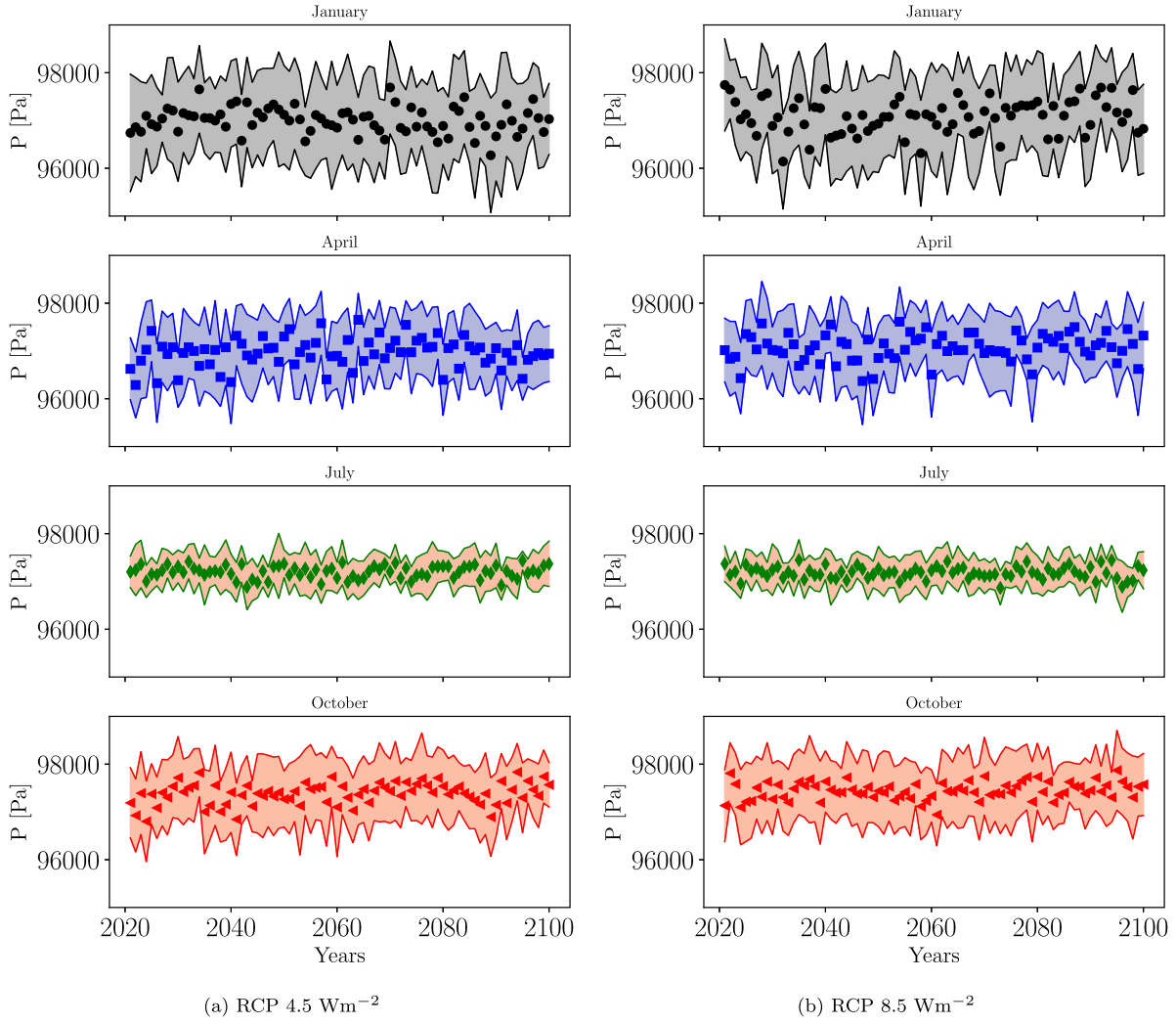

Fig. 12. Future climate pressure time series for (a) RCP 4.5 Wm^{-2} and (b) RCP 8.5 Wm^{-2}; the markers and shaded region showing the mean and one standard deviation, respectively, for annual daily values produced by the created future EnergyPlus Weather (EPW) weather file; showing selected months of January, April, July, and October.

over time (~15–30% for RCP 4.5–8.5 Wm^{-2}) and the building sensible cooling demand is increased over time (~20–50% for RCP 4.5–8.5 Wm^{-2}). The amount of change is greater for RCP 8.5 than RCP 4.5 Wm^{-2}. For RCP 4.5 Wm^{-2} there is an anomaly for building sensible cooling demand in year 2090, which shows a substantial reduction compared to the previous and next decade. This anomaly is consistent with Fig. 10a, which also shows a temporary cooling effect on temperature around 2090s for the selected months.

The results provided by VWFG and VCWG can be compared with some other investigations. For instance, Troup et al. [8] studied an office buildings in Boston, U.S.A, using EnergyPlus for future climate impacts on building energy demand from the current climate until 2090s. They used an ensemble of fourteen Global Climate Models (GCMs) and two Representative Concentration Pathways (RCPs) of 4.5 and 8.5 Wm^{-2} for statistical downscaling and morphing of weather files into the future. They found that the increase in building energy consumption is dominated by increasing cooling demand of about 10%.

D'Agostino et al. [7] studied building energy demands of various European cities from the present time to 2060 using a weather file dataset created via morphing with the application of the WeatherShift™ tool, considering the RCP 8.5 Wm^{-2} scenario. They focused on two-story residential buildings, and conducted the building energy analysis using EnergyPlus. They reported a heating demand decrease of 38–57% and a cooling demand increase of 90–380% by 2060.

Bamdad et al. [4] studied building energy demands of two Australian cities, Brisbane and Canberra, from the present time to 2080 using a weather file dataset created via morphing with the application of the CCWorldWeatherGen tool, considering the A2 emission scenario from the Fourth Assessment Report of IPCC. This scenario accounts for continuously increasing global population with regionally oriented economic development, and slower technological change. They focused on a multi-story Type B building and

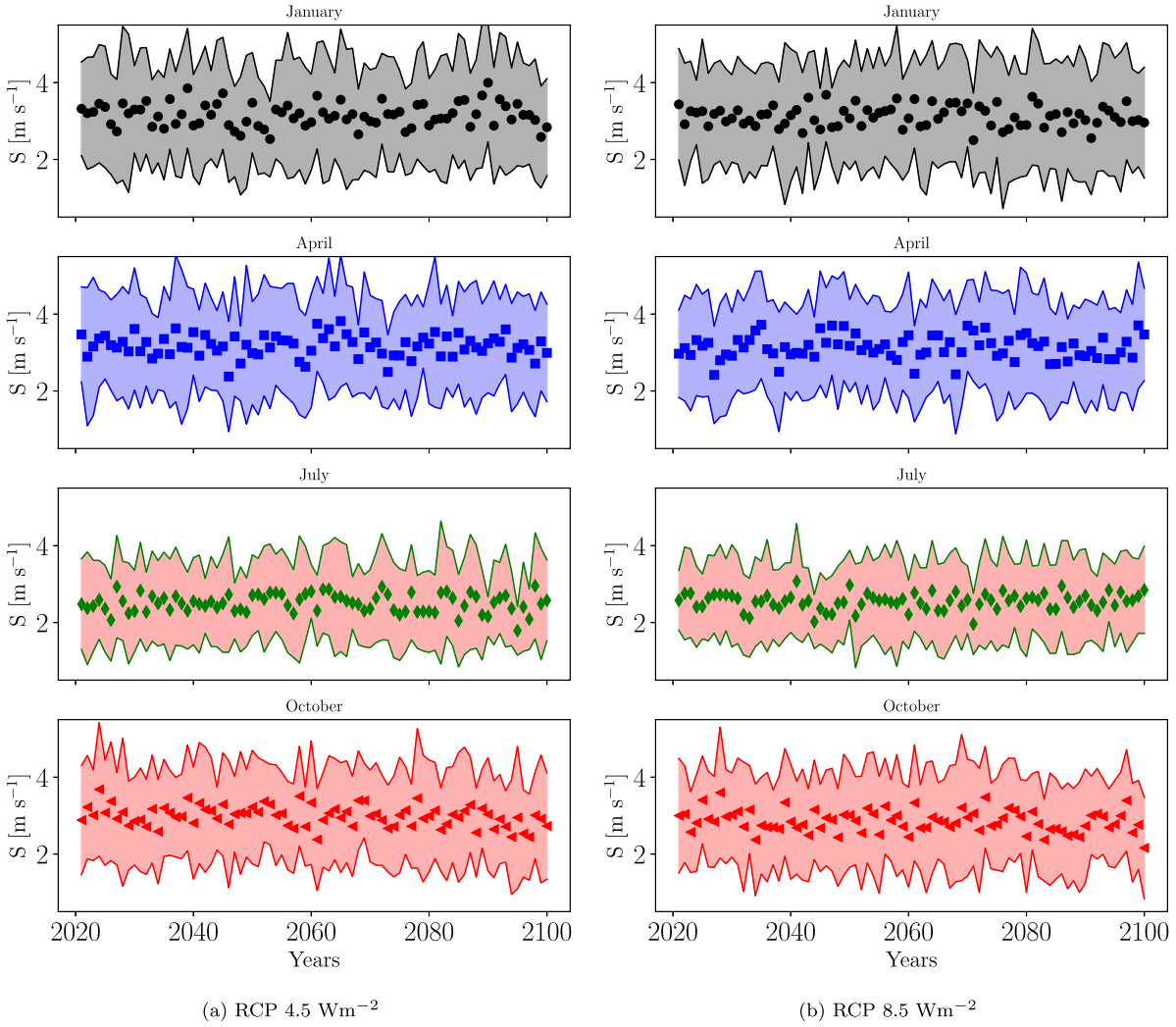

Fig. 13. Future climate wind speed time series for (a) RCP 4.5 Wm^{-2} and (b) RCP 8.5 Wm^{-2}; the markers and shaded region showing the mean and one standard deviation, respectively, for annual daily values produced by the created future EnergyPlus Weather (EPW) weather file; showing selected months of January, April, July, and October.

used the EnergyPlus for building energy analysis. In both cities, no substantial change in the building heating demand is predicted, but an increase of ~30% in building cooling demand is predicted by 2080.

In another study, P. Tootkaboni et al. [3] investigated the building energy demand for Rome, Italy, from the present time to 2050 using three weather generator tools: WeatherShift™, CCWorldWeatherGen, and Meteonorm, considering the RCP 8.5 Wm^{-2} scenario. They focused on multi-story residential buildings, and conducted the building energy analysis using EnergyPlus. All the weather generator tools used the statistical downscaling approach and provided similar results. They reported a heating demand decrease of ~25% and a cooling demand increase of ~35% by 2050.

The VWFG and VCWG results are in agreement with previous studies mentioned above, so that in most locations with future climates considered, the decrease in building heating demand is less than the increase in building cooling demand. The specific quantitative values may change given the simulation tools used, future climate scenario, building type, and the region of interest.

4. Conclusions and future work

Urban physics models require reliable weather files for future climate scenario simulations. Two common approaches to produce such files are statistical and dynamical downscaling methods. While statistical downscaling can be computationally fast, it can be less accurate than the computationally expensive dynamical downscaling method.

Current statistical downscaling methods are based on the morphing technique, in which the statistics of future weather variables (e.g. mean and standard deviation) are matched by selecting and manipulating historical weather files at high temporal resolution,

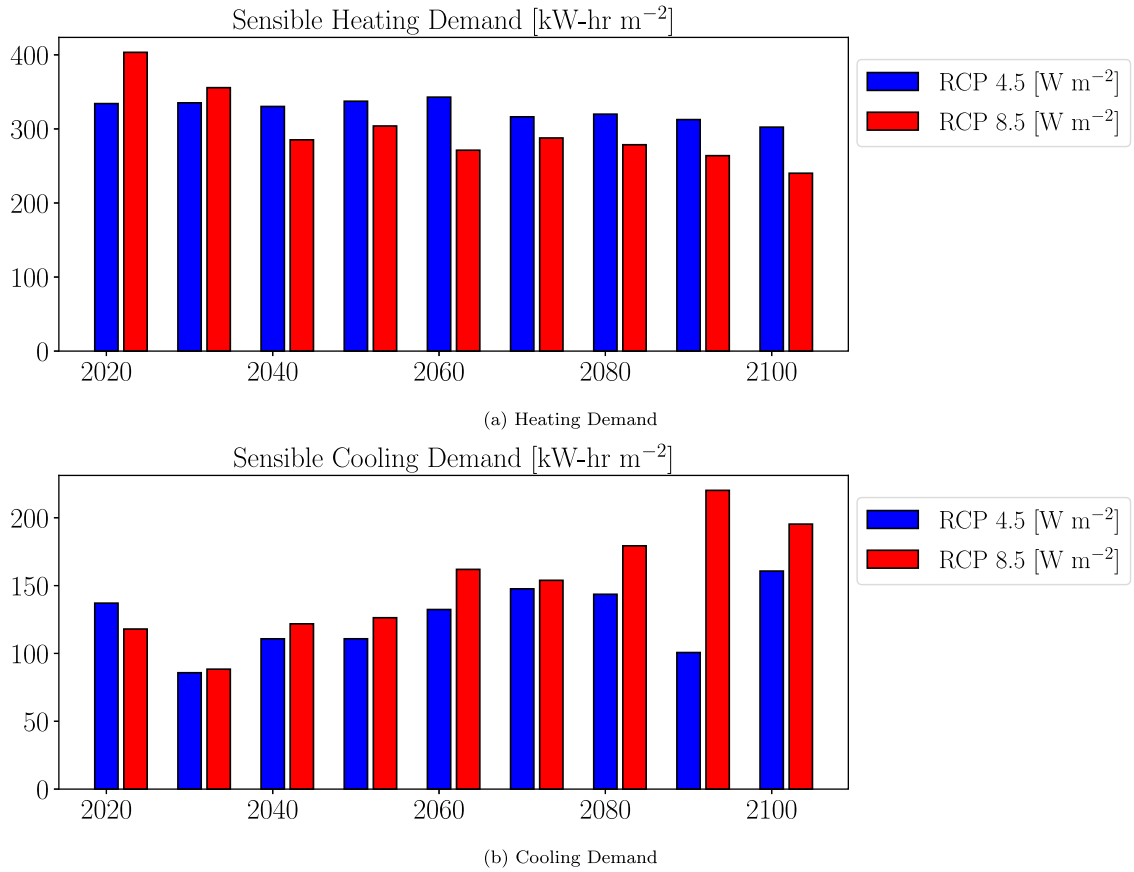

Fig. 14. Annual building energy demand for (a) sensible heating and (b) sensible cooling for RCP 4.5 and 8.5 Wm^{-2}.

so that future weather files can be generated. Multiple tools are available for general use based on the statistical downscaling technique, such as WeatherShift™, CCWorldWeatherGen, and Meteonorm.

Despite the advances, several gaps remain in development of statistical downscaling methods for weather file generation: (1) lack of flexibility in the driving datasets that are used in a tool, such as the choice of Climate Model (CM) and the historical weather files based on observations or reanalysis data products, (2) lack of consideration for selecting the historical weather files over an extended period of time (at least two decades), instead of relying on only a few Typical Meteorological Year (TMY) or eXtreme Meteorological Year (XMY) files, (3) lack of flexibility in the choice of the number of meteorological variables for statistical analysis (e.g. dry bulb temperature, wind speed, etc.), and (4) lack of simplicity.

In this study a new weather file generator is proposed. Titled the Vatic Weather File Generator (VWFG), this tool overcomes the previous difficulties in future weather file generators based on the statistical downscaling technique. The VWFG (1) applies a bias correction procedure on a quantile–quantile basis to improve the validation or future CM records; (2) employs the Finkelstein–Schafer (F-S) statistic on a quantile–quantile basis to match the validation or future CM records to the corresponding historical weather file records; and (3) applies the shifting–stretching technique to monthly distributions of historical weather data so they match with the validation or future climate variable means and standard deviations.

This implementation of the VWFG is forced by the CanRCM4 model as CM records and the ERA5 reanalysis data product as the weather file records. The historical period is 1980–1999, the validation period is 2007–2020, and the future period is 2021–2100. The climate of Toronto, Canada, is analyzed under Representative Concentration Pathway (RCP) scenarios of 4.5 and 8.5 Wm^{-2}. Further, an urban physics models, titled the Vertical City Weather Generator (VCWG), is forced by the output of VWFG to predict the building sensible heating and cooling demands for a two-story single-family residential house in Toronto. The outcome of the analysis suggests that the building sensible heating demand is reduced over time (~15–30% for RCP 4.5–8.5 Wm^{-2}) and the building sensible cooling demand is increased over time (~20–50% for RCP 4.5–8.5 Wm^{-2}) by 2100. The amount of change is greater for RCP 8.5 than RCP 4.5 Wm^{-2}.

VWFG has practical implications for creating future weather files to force urban physics simulations under different future climate scenarios. Users of VWFG will have a very flexible platform that is easy to utilize and widely applicable to generate the required weather files for any geographic location, time period, and future scenario of interest. This is particularly helpful where limited weather observations are available, standard tools are not flexible, or dynamical downscaling of future climate models is not feasible.

Future work shall entail application of VWFG in different locations and various climate zones. VWFG's performance can also be assessed by considering various forcing datasets and different choices of meteorological variables. Using VWFG, various building energy retrofit options can be investigated to understand which alternative and renewable energy systems can reduce the environmental impact of urban areas in future climates.

CRediT authorship contribution statement

Amir A. Aliabadi: Conceptualization, Formal analysis, Investigation, Methodology, Model comparison, Visualization, Writing – original draft, Funding acquisition, Supervision, Writing – review & editing. **Rachel M. McLeod:** Data curation, Formal analysis, Investigation, Writing – review & editing.

Declaration of competing interest

The authors declare that they have no known competing financial interests or personal relationships that could have appeared to influence the work reported in this paper.

Data availability

The Vatic Weather File Generator (VWFG v1.0.0) is accessible online via https://github.com/AmirAAliabadi.

Acknowledgments

The authors are indebted to Amanda Sawlor, Datev Dodkelian, Esra Mohamed, Di Cheng, Randy Regan, Margaret Love, and Angela Vuk at the University of Guelph for administrative support. The computational platforms were set up with the assistance of IT staff Matthew Kurylo, Jeff Madge, Joel Best, and Matthew Kent at the University of Guelph. The authors thank the assistance of Mohsen Moradi, who developed the initial algorithms to retrieve ERA5 data products toward the creation of EnergyPlus Weather (EPW) files.

This work was supported by the University of Guelph; the Discovery Grant program (401231) from the Natural Sciences and Engineering Research Council (NSERC) of Canada; Government of Ontario through the Ontario Centres of Excellence (OCE) under the Alberta-Ontario Innovation Program (AOIP) (053450); Emission Reduction Alberta (ERA) (053498); Accelerate program (460847) from the Mathematics of Information Technology and Complex Systems (MITACS); and Blue Valley Building Corp. OCE is a member of the Ontario Network of Entrepreneurs (ONE).

References

[1] H.-O. Pörtner, D.C. Roberts, H. Adams, et al., Technical summary, in: H.-O. Pörtner, D.C. Roberts, E.S. Poloczanska, et al. (Eds.), Climate Change 2022: Impacts, Adaptation and Vulnerability. Contribution of Working Group II to the Sixth Assessment Report of the Intergovernmental Panel on Climate Change, Cambridge University Press, Cambridge and New York, 2022, pp. 37–118, http://dx.doi.org/10.1017/9781009325844.002.

[2] A. Moazami, V.M. Nik, S. Carlucci, S. Geving, Impacts of future weather data typology on building energy performance – investigating long-term patterns of climate change and extreme weather conditions, Appl. Energy 238 (2019) 696–720, http://dx.doi.org/10.1016/j.apenergy.2019.01.085.

[3] M. P. Tootkaboni, I. Ballarini, M. Zinzi, V. Corrado, A comparative analysis of different future weather data for building energy performance simulation, Climate 9 (2) (2021) 37, http://dx.doi.org/10.3390/cli9020037.

[4] K. Bamdad, M.E. Cholette, S. Omrani, J. Bell, Future energy-optimised buildings — Addressing the impact of climate change on buildings, Energy Build. 231 (2021) 110610, http://dx.doi.org/10.1016/j.enbuild.2020.110610.

[5] S.E. Belcher, J.N. Hacker, D.S. Powell, Constructing design weather data for future climates, Build. Serv. Eng. Res. Technol. 26 (1) (2005) 49–61, http://dx.doi.org/10.1191/0143624405bt112oa.

[6] M.F. Jentsch, A.S. Bahaj, P.A. James, Climate change future proofing of buildings—Generation and assessment of building simulation weather files, Energy Build. 40 (12) (2008) 2148–2168, http://dx.doi.org/10.1016/j.enbuild.2008.06.005.

[7] D. D'Agostino, D. Parker, I. Epifani, D. Crawley, L. Lawrie, How will future climate impact the design and performance of nearly zero energy buildings (NZEBs)? Energy 240 (2022) 122479, http://dx.doi.org/10.1016/j.energy.2021.122479.

[8] L. Troup, M.J. Eckelman, D. Fannon, Simulating future energy consumption in office buildings using an ensemble of morphed climate data, Appl. Energy 255 (2019) 113821, http://dx.doi.org/10.1016/j.apenergy.2019.113821.

[9] M. Hosseini, A. Bigtashi, B. Lee, Generating future weather files under climate change scenarios to support building energy simulation - a machine learning approach, Energy Build. 230 (2021) 110543, http://dx.doi.org/10.1016/j.enbuild.2020.110543.

[10] M. Herrera, S. Natarajan, D.A. Coley, T. Kershaw, A.P. Ramallo-González, M. Eames, D. Fosas, M. Wood, A review of current and future weather data for building simulation, Build. Serv. Eng. Res. Technol. 38 (5) (2017) 602–627, http://dx.doi.org/10.1177/0143624417705937.

[11] M. Zhu, Y. Pan, Z. Huang, P. Xu, An alternative method to predict future weather data for building energy demand simulation under global climate change, Energy Build. 113 (2016) 74–86, http://dx.doi.org/10.1016/j.enbuild.2015.12.020.

[12] M.F. Jentsch, P.A. James, L. Bourikas, A.S. Bahaj, Transforming existing weather data for worldwide locations to enable energy and building performance simulation under future climates, Renew. Energy 55 (2013) 514–524, http://dx.doi.org/10.1016/j.renene.2012.12.049.

[13] H. Hersbach, B. Bell, P. Berrisford, S. Hirahara, A. Horányi, J. Muñoz-Sabater, J. Nicolas, C. Peubey, R. Radu, D. Schepers, A. Simmons, C. Soci, S. Abdalla, X. Abellan, G. Balsamo, P. Bechtold, G. Biavati, J. Bidlot, M. Bonavita, G. De Chiara, P. Dahlgren, D. Dee, M. Diamantakis, R. Dragani, J. Flemming, R. Forbes, M. Fuentes, A. Geer, L. Haimberger, S. Healy, R.J. Hogan, E. Hólm, M. Janisková, S. Keeley, P. Laloyaux, P. Lopez, C. Lupu, G. Radnoti, P. de Rosnay, I. Rozum, F. Vamborg, S. Villaume, J.-N. Thépaut, The ERA5 global reanalysis, Q. J. R. Meteorol. Soc. 146 (730) (2020) 1999–2049, http://dx.doi.org/10.1002/qj.3803.

[14] B. Bueno, L.K. Norford, G. Pigeon, R. Britter, Combining a detailed building energy model with a physically-based urban Canopy model, Bound.-Lay. Meteorol. 140 (3) (2011) 471–489, http://dx.doi.org/10.1007/s10546-011-9620-6.

[15] B. Bueno, L. Norford, J. Hidalgo, G. Pigeon, The urban weather generator, J. Build. Perf. Simulat. 6 (4) (2012) 269–281, http://dx.doi.org/10.1080/19401493.2012.718797.
[16] B. Bueno, G. Pigeon, L.K. Norford, K. Zibouche, C. Marchadier, Development and evaluation of a building energy model integrated in the TEB scheme, Geosci. Model Dev. 5 (3) (2012) 433–448, http://dx.doi.org/10.5194/gmd-5-433-2012.
[17] B. Bueno, M. Roth, L.K. Norford, R. Li, Computationally efficient prediction of canopy level urban air temperature at the neighbourhood scale, Urban Clim. 9 (2014) 35–53, http://dx.doi.org/10.1016/j.uclim.2014.05.005.
[18] A.A. Aliabadi, M. Moradi, R.M. McLeod, D. Calder, R. Dernovsek, How much building renewable energy is enough? The vertical city weather generator (VCWG v1.4.4), Atmosphere 12 (7) (2021) 882, http://dx.doi.org/10.3390/atmos12070882.
[19] M. Moradi, B. Dyer, A. Nazem, M.K. Nambiar, M.R. Nahian, B. Bueno, C. Mackey, S. Vasanthakumar, N. Nazarian, E.S. Krayenhoff, L.K. Norford, A.A. Aliabadi, The vertical city weather generator (VCWG v1.3.2), Geosci. Model Dev. 14 (2) (2021) 961–984, http://dx.doi.org/10.5194/gmd-14-961-2021.
[20] M. Moradi, E.S. Krayenhoff, A.A. Aliabadi, A comprehensive indoor–outdoor urban climate model with hydrology: The vertical city weather generator (VCWG v2.0.0), Build. Environ. 207 (2022) 108406, http://dx.doi.org/10.1016/j.buildenv.2021.108406.
[21] A. Zadra, D. Caya, J. Côté, B. Dugas, C. Jones, R. Laprise, K. Winger, L.-P. Caron, The next Canadian regional climate model, Phys. Canada 64 (2) (2008) 75–83.
[22] J.F. Scinocca, V.V. Kharin, Y. Jiao, M.W. Qian, M. Lazare, L. Solheim, G.M. Flato, S. Biner, M. Desgagne, B. Dugas, Coordinated global and regional climate modeling, J. Clim. 29 (1) (2016) 17–35, http://dx.doi.org/10.1175/JCLI-D-15-0161.1.
[23] G. Krinner, M.G. Flanner, Striking stationarity of large-scale climate model bias patterns under strong climate change, Proc. Natl. Acad. Sci. USA 115 (38) (2018) 9462–9466, http://dx.doi.org/10.1073/pnas.1807912115.
[24] K.W. Dixon, J.R. Lanzante, M.J. Nath, K. Hayhoe, A. Stoner, A. Radhakrishnan, V. Balaji, C.F. Gaitán, Evaluating the stationarity assumption in statistically downscaled climate projections: Is past performance an indicator of future results? Clim. Change 135 (2016) 395–408, http://dx.doi.org/10.1007/s10584-016-1598-0.
[25] J.R. Lanzante, K.W. Dixon, M.J. Nath, C.E. Whitlock, D. Adams-Smith, Some Pitfalls in statistical downscaling of future climate, Bull. Am. Meteorol. Soc. 99 (4) (2018) 791–803, http://dx.doi.org/10.1175/BAMS-D-17-0046.1.
[26] A. Amengual, V. Homar, R. Romero, S. Alonso, C. Ramis, A statistical adjustment of regional climate model outputs to local scales: Application to platja de palma, Spain, J. Clim. 25 (3) (2012) 939–957, http://dx.doi.org/10.1175/JCLI-D-10-05024.1.
[27] M. Hosseini, A. Bigtashi, B. Lee, A systematic approach in constructing typical meteorological year weather files using machine learning, Energy Build. 226 (2020) 110375, http://dx.doi.org/10.1016/j.enbuild.2020.110375.
[28] A.A. Aliabadi, M. Moradi, D. Clement, W.D. Lubitz, B. Gharabaghi, Flow and temperature dynamics in an urban canyon under a comprehensive set of wind directions, wind speeds, and thermal stability conditions, Environ. Fluid Mech. 19 (1) (2019) 81–109, http://dx.doi.org/10.1007/s10652-018-9606-8.
[29] E.S. Krayenhoff, T. Jiang, A. Christen, A. Martilli, T.R. Oke, B.N. Bailey, N. Nazarian, J.A. Voogt, M.G. Giometto, A. Stastny, B.R. Crawford, A multi-layer urban canopy meteorological model with trees (BEP-tree): Street tree impacts on pedestrian-level climate, Urban Clim. 32 (2020) 100590, http://dx.doi.org/10.1016/j.uclim.2020.100590.
[30] A.A. Aliabadi, M. Moradi, R.A.E. Byerlay, The budgets of turbulence kinetic energy and heat in the urban roughness sublayer, Environ. Fluid Mech. 21 (4) (2021) 843–884, http://dx.doi.org/10.1007/s10652-021-09800-x.
[31] M.R. Nahian, A. Nazem, M.K. Nambiar, R. Byerlay, S. Mahmud, A.M. Seguin, F.R. Robe, J. Ravenhill, A.A. Aliabadi, Complex meteorology over a complex mining facility: Assessment of topography, land use, and grid spacing modifications in WRF, J. Appl. Meteorol. Climatol. 59 (4) (2020) 769–789, http://dx.doi.org/10.1175/JAMC-D-19-0213.1.
[32] M.K. Nambiar, R.A.E. Byerlay, A. Nazem, M.R. Nahian, M. Moradi, A.A. Aliabadi, A tethered air blimp (TAB) for observing the microclimate over a complex terrain, Geosci. Instrum. Meth. Data Syst. 9 (1) (2020) 193–211, http://dx.doi.org/10.5194/gi-9-193-2020.
[33] M.K. Nambiar, F.R. Robe, A.M. Seguin, M. Endsin, A.A. Aliabadi, Diurnal and seasonal variation of area-fugitive methane advective flux from an open-pit mining facility in northern Canada using WRF, Atmosphere 11 (11) (2020) 1227, http://dx.doi.org/10.3390/atmos11111227.
[34] S. Kia, M.K. Nambiar, J. Thé, B. Gharabaghi, A.A. Aliabadi, Machine learning to predict area fugitive emission fluxes of GHGs from open-pit mines, Atmosphere 13 (2) (2022) 210, http://dx.doi.org/10.3390/atmos13020210.
[35] S. Kia, T.K. Flesch, B.S. Freeman, A.A. Aliabadi, Calculating gas emissions from open-pit mines using inverse dispersion modelling: A numerical evaluation using CALPUFF and CFD-LS, J. Wind. Eng. Ind. Aerodyn. 226 (2022) 105046, http://dx.doi.org/10.1016/j.jweia.2022.105046.
[36] A.A. Aliabadi, Turbulence: A Fundamental Approach for Scientists and Engineers, Springer, Cham, 2022, http://dx.doi.org/10.1007/978-3-030-95411-6.